



Full length article

Chemical bonding effects on the brittle-to-ductile transition in metallic glasses

F. Moitzi^a, D. Şopu^{a,b,*}, D. Holec^c, D. Perera^b, N. Mousseau^d, J. Eckert^{a,e}

^a Erich Schmid Institute of Materials Science, Austrian Academy of Sciences, Jahnstraße 12, Leoben 8700, Austria

^b Institut für Materialwissenschaft, Technische Universität Darmstadt, Otto-Berndt-Straße 3, Darmstadt 64287, Germany

^c Department of Materials Science, Chair of Physical Metallurgy and Metallic Materials, Montanuniversität Leoben, Roseggerstraße 12, Leoben 8700, Austria

^d Département de Physique and Regroupement Québécois sur les Matériaux de Pointe, Université de Montréal Canada

^e Department of Materials Science, Chair of Material Physics, Montanuniversität Leoben, Jahnstraße 12, Leoben 8700, Austria

ARTICLE INFO

Article History:

Received 19 December 2019

Revised 31 January 2020

Accepted 1 February 2020

Available online 10 February 2020

Keywords:

Molecular dynamics

Density functional theory

Crystal orbital hamiltonian population

Metallic glasses

PdSi

Shear bands

Cracks

Plasticity

ABSTRACT

The influence of composition and temperature on the tensile deformation behavior of amorphous PdSi metal-metalloid alloys is investigated using large-scale molecular dynamics simulations. A correlation between highly directional Si-Si bonds and the deformation mechanisms is revealed by a Crystal Orbital Hamilton Population analysis based on electronic structure calculations from density functional theory. A transition from cracking perpendicular to the loading direction to shear banding can be achieved by increasing the temperature or decreasing the amount of silicon. Sampling of the saddle points on the potential energy surface reveals that a high fraction of rigid covalent Si-Si bonds increases the energy barriers for atomic rearrangements. These thermally-activated atomic relaxation events change the stress and strain state in the elastic regime and are precursor of local plasticity. High activation energies impede both the stress and the strain redistribution and cause cleavage-like cracking due to a delay of the onset of plasticity.

© 2020 Acta Materialia Inc. Published by Elsevier Ltd. All rights reserved.

1. Introduction

The possibility of a high yield strength similar to engineering ceramics but with superior toughness has inspired substantial research efforts on the room-temperature properties of metallic glasses (MG) [1]. Some MGs exhibit pronounced plasticity under compressive loading, whereas under tensile loading, a sudden catastrophic failure is observed due to either highly localized narrow shear band formation [2,3] or cracking perpendicular to the loading direction [4]. The failure behavior limits the applicability of MGs as advanced materials since the impending failure is not prior noticeable. Considerable efforts have been done to address these problems systematically by correlating the mechanical properties with the structure [5]. However, the structure-property relationships are experimentally challenging to investigate because of the amorphous nature of MGs and the spatial and temporal scales of the deformation processes [6]. The currently accessible sample sizes and timescales of molecular dynamics simulations (MD) are ideal for studying the atomic rearrangements during deformation of MGs. Additionally,

numerous physical properties and structural descriptors are directly accessible that can be used to explain the mechanical properties and the deformation behavior of MGs; activation energy barriers in the potential energy landscape [5,7] or structural-based signatures like short-range or medium-range order [8], bond length deviation [9], flexibility volume [10], to name just a few, have been correlated to the onset of plasticity in MGs. Nevertheless, the explanatory power of MD simulations relies heavily on the generated thermodynamic state, specifically the relaxation state in MG, and on the adequate use of the interatomic potentials within the restricted domain of application, where the physical approximations are still correct. While the most commonly used interatomic potentials for MGs reproduce their atomic topology and structure correctly, their dynamic behavior deviates from experimental findings. Especially, for tensile MD simulations of MGs cracking is absent, which contradicts with experiment [11]. An exception to the rule is the work of Murali et al. [12] where cracking in the FeP glass was reported due to atomic-scale spatial fluctuations in the local properties. However, one should mention that the potential involved in this work was not designed to mimic realistic phase behavior of the amorphous phase. Furthermore, the interatomic potential did not include covalent interactions and the system was extremely unstable to spinodal decomposition leading to segregated phases. This eliminates the transferability to comparable

* Corresponding author at: Erich Schmid Institute of Materials Science, Austrian Academy of Sciences, Jahnstraße 12, 8700 Leoben, Austria.

E-mail address: daniel.sopu@oeaw.ac.at (D. Şopu).

experimental MG systems [13] and contradicts the finding that MGs containing two glassy phases have substantial plasticity [14]. Hence, a systematic atomic-level understanding of the empirically observed embrittlement in metal-metalloid glasses is still lacking and further studies need to be undertaken to explore the fracture mechanism. The aim of this study is to investigate the relationship between the deformation behavior of metal-metalloid glasses and their intrinsic properties by performing tensile simulations using large-scale MD simulations with hybrid interatomic potentials including the many-body potential Embedded Atom Method (EAM) [15] and Bond-Order potential [16] calculations. A quantitative interpretation of the observed deformation mechanisms is provided by sampling the potential energy surface for the energy barrier of local atomic rearrangements with the activation-relaxation technique (ART) [17–19]. Since inherent brittleness is suspected to be connected to covalent hybridized bonds [20], a chemical bond analysis based on electronic structure calculations from density functional theory (DFT) is performed and the interatomic potential is selected based on the findings. For this study, the bonding is categorized based on spatial distribution and localization of the electron density and their energetic behavior using Crystal Orbital Hamilton Population Analysis (COHP). The fracture behavior is evaluated by accounting for covalent interactions on the deformation mechanism. Finally, the experimentally known macroscopic deformation behavior is compared to the atomistic mechanism observed in the simulations.

2. Simulation approach

Tensile simulations and preceding sample preparation was carried out with the large-scale molecular dynamics simulation software LAMMPS [21]. The Pd-Pd and Pd-Si interactions were treated with an EAM potential developed by Sheng et al. [15], while the Si-Si interactions were treated by an angular dependent Tersoff potential [16]. A different approach was used for creating the starting sample as compared to the usual method consisting of relaxing very slowly a small cell, which is then repeated periodically [22]. The intention was to remove any periodicity of structural identities, which can bias results of stress analysis. The starting liquid structure was created, therefore, by randomly distributing 968,000 atoms in a box of $111.0 \times 55.5 \times 2.5$ nm with periodic boundary conditions. The z-direction was chosen as thin as possible still taking into account the potential cutoff of 6.5 Å and ensuring that distribution of Voronoi polyhedron and bond angles are not affected. Uniform-acceptance force bias Monte Carlo [23] and MD in an *NPT* ensemble were used alternately, in order to deal with the overlap between the atoms during the initial equilibration of the liquid structure. Then, the samples were cooled down 50 K above T_g at a rate of 10 K/ps starting from 1600 K. The glass transition temperature T_g lies for Pd₈₀Si₂₀, Pd₅₀Si₅₀ and Pd₃₅Si₆₅ at 850 K, 1150 K and 1250 K, respectively. The important cooling process to get a well-relaxed structure is in a temperature range of 100 K [24] and was therefore performed at a rate of 0.02 K/ps. After cooling down 50 K below T_g an annealing for 4.0 ns was performed. The final cooling to 50 K was then done with 10 K/ps. The cooled-down sample was replicated twice along the z-direction. Thereafter, the sample was notched on both sides to get a symmetric and well-defined stress state and deformation site. The size and the geometry of the notches were chosen in a way that shear banding occurs [25,26]. Open boundaries in y-direction and periodic boundaries in the x- and z-directions were applied. Lastly, the sample was relaxed for 0.2 ns to reach 0 GPa overall pressure. The tensile simulations were performed under a constant engineering strain rate of 0.00004 ps^{-1} . The integration time step was 2 fs. A barostat was applied in the z-direction only, which led to a plane stress state in the sample. The box was deformed every 1 ps timesteps and the coordinates were remapped according to an affine transformation. Elastic constants were obtained by applying small strains and sampling the stress response in an *NVE* ensemble. The strain was chosen small enough not to introduce plastic deformation and to violate definition of the elastic constants at

zero strain and big enough not to be affected by statistical fluctuations [27]. The linear elastic coefficients were calculated from this stress response and deformation. Always starting from the initial structure the box was extended, compressed or sheared by 1.5% and the stress difference after 5 ps was measured. This was carried out for 25 different starting velocity distributions in order to minimize the statistical error. The obtained elastic coefficients were averaged over these runs. The results of the MD simulations were analyzed with OVITO [28]. MD offers the possibility to investigate dynamical processes on the atomic scale qualitatively. However, an analysis of the actual chemical bonding can only reliably be obtained from ab-initio electronic structure methods. By using a supercell approach, DFT gives quantitative access to the energy of metastable structures and states, and the correlation between bond energy density and elastic properties of MGs. The resulting spatial distribution of the electronic structure can be used for a physically motivated selection of the interatomic potential. The initial supercooled structure of 120 atoms was created by an MD simulation in LAMMPS. For further relaxation, an ab-initio MD anneal run for 300 fs with a time step of 1 fs was then performed using SIESTA [29]. A polarization double zeta basis set was used with an energy shift of 100 meV. The mesh cutoff was set to 200.0 Ry. K-point sampling was done with a Monkhorst-Pack scheme with $3 \times 3 \times 3$ points and a shift of (0.5, 0.5, 0.5) in order to reduce the number of equivalent k-points. The exchange-correlation functional was GGA-PBE [30]. The pseudopotentials for Pd and Si were taken from the SIESTA pseudopotential database [31]. The DFT calculations were analyzed with COHP [32], ASE [33] and XCrySDen [34]. The Activation-Relaxation Technique (ART) [17–19] offers a way to locally sample the energy landscape and quantify activation pathways between adjacent minima energetically [7]. The distribution of activation energies can be correlated with the probability of thermally and stress activated relaxation phenomena [10]. Two starting structures of Pd₈₀Si₂₀ and Pd₃₅Si₆₅ with 4000 atoms were created following the above mentioned procedure. The system was then relaxed to zero kinetic energy with global interatomic forces minimized to 10^{-6} eV/Å . For each atom in this structure, 10 relaxation pathways were searched with ART, always starting from the same initial structure. These events are then characterized as function of energy, in particular, for atoms with a displacement bigger than 0.1 Å. Special emphasis was given to the low-energy local atomic relaxations at energies below 0.2 eV and not diffusional jumps which have higher energy at around 3 eV and larger atomic displacements.

3. Results

3.1. Interatomic potential selection from the electronic structure

Existing interatomic potentials for the amorphous metal-metalloid system suffer from qualitative flaws in describing the actual deformation in metallic glasses on the atomic scale [13]. One of the problems arises from a fundamental error in the potential design: the failure to describe short-range covalent bonding of the silicon electrons. Thus, in the present work the interatomic potential was extended with a three-body term for the Si-Si interactions to ensure a more accurate description of the covalent interactions. A chemical bond analysis for different compositions was performed in order to validate this approach. Firstly, the spatial distribution of the electronic density was investigated for Pd₅₀Si₅₀ to identify any charge localization and accumulation. The difference between self-consistent and atomic charge density (Fig. 1 (A)) shows in general lowered electron density around atomic sites and specifically pronounced charge accumulation between Si-Si first neighbors, which is a strong evidence for covalent bond formation between the Si-Si atoms. Furthermore, plotting the electron density for distinctive bonding regions in the Crystal Orbital Hamiltonian Population (COHP) curves (Fig. 2), we observe that strongly directional bonds are formed by partially filling the overlapped atomic orbitals of Si (Fig. 1 B.I and Fig. 1 B.II). The bonds between Pd and Si are less localized and even polarized towards the Pd atoms (Fig. 1 B.II). The COHP curves show that

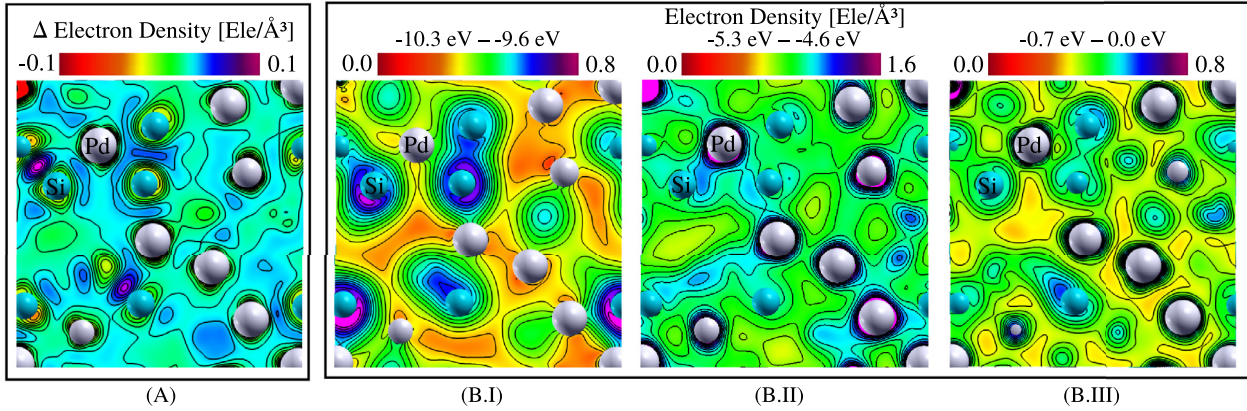


Fig. 1. Difference between self-consistent and atomic charge density (A) and charge density at different energy ranges for Pd₅₀Si₅₀ (B.I-III). (A) shows strong charge accumulation between the Si atoms. (B.I) and (B.III) show covalent bond formation of the silicon atoms. (B.II) shows polarized and weak covalent bonds between Si and Pd.

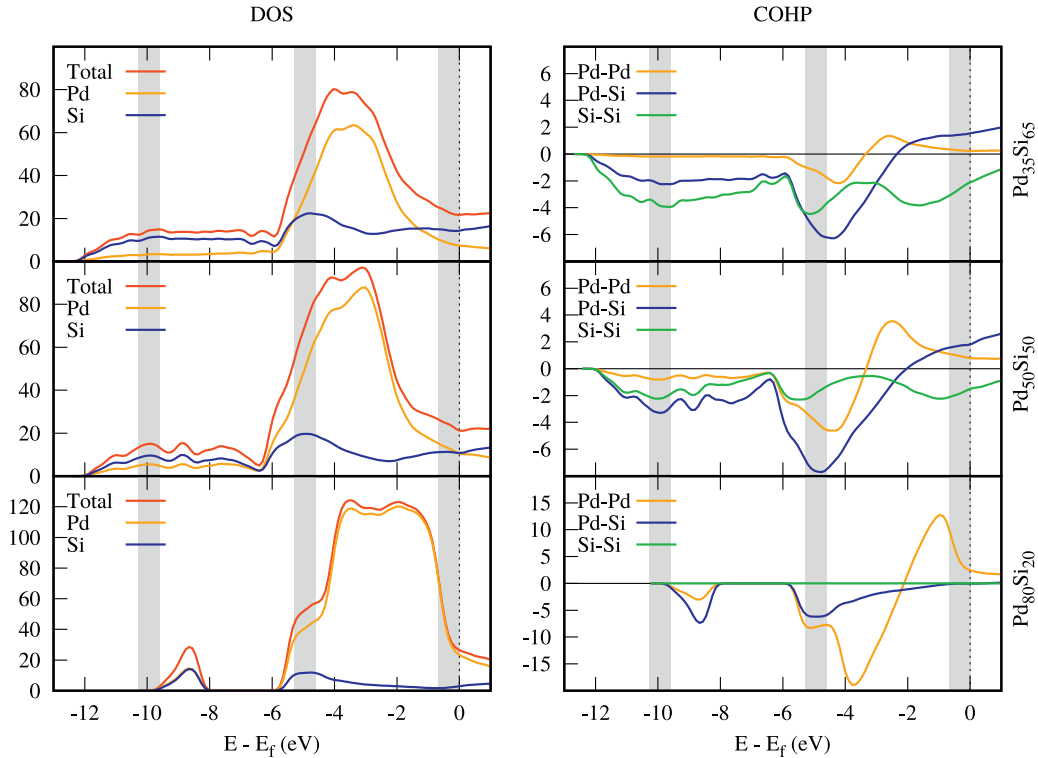


Fig. 2. DOS and COHP curves [Ry/eV] for different compositions of PdSi. The Fermi energy is at 0 eV. The spatial distribution of the electron density of the grey marked energy ranges is shown in Fig. 1.

the Si-Si interactions are bonding within the whole valence band (Fig. 2). The vanishing Si-Si COHP curve in Pd₈₀Si₂₀ results from the absence of Si around the nearest neighbor shell of a silicon atom and, therefore, an absence of short-range covalent bonding. The sinusoidal shape of the Pd-Pd COHP curve at around -5 to -1 eV indicates non-bonding overall interactions in Pd-Pd. The Pd-Si COHP curves from around -2 eV are antibonding. This electronic instability near the Fermi level of the system is due to the unfavorable amorphous structure [32]. Moreover, a non-zero density of states at the Fermi level indicates a metallic character. A more quantitative analysis can be done by integrating the COHP curves up to the Fermi level and normalize them per bond. The integrated COHP (ICOHP) curves can be found in Table 1. The resulting values for the Si-Si orbital interactions are strongly negative and can be a measure for the real bond energies [20]. Schnabel et. al [35]

Table 1

Integrated COHP curves (ICOHP) for Pd₃₅Si₆₅, Pd₅₀Si₅₀ and Pd₈₀Si₂₀. The number of bonds was obtained between a cutoff of $r_{min} = 2.0 \text{ \AA}$ and $r_{max} = 3.4 \text{ \AA}$.

ICOHP per Bond [eV]	Pd ₃₅ Si ₆₅	Pd ₅₀ Si ₅₀	Pd ₈₀ Si ₂₀
Pd-Pd	-0.66	-0.48	-0.67
Pd-Si	-1.00	-1.00	-1.23
Si-Si	-3.17	-2.45	0.00

found that the presence of covalent bonds and hybridization correlate with the reduction of toughness and embrittlement in metallic glasses. The highly negative ICOHP values and the pronounced charge accumulation are strong evidence for covalent bonding interactions between the Si-Si atoms. The presence of these interactions is the physical motivation

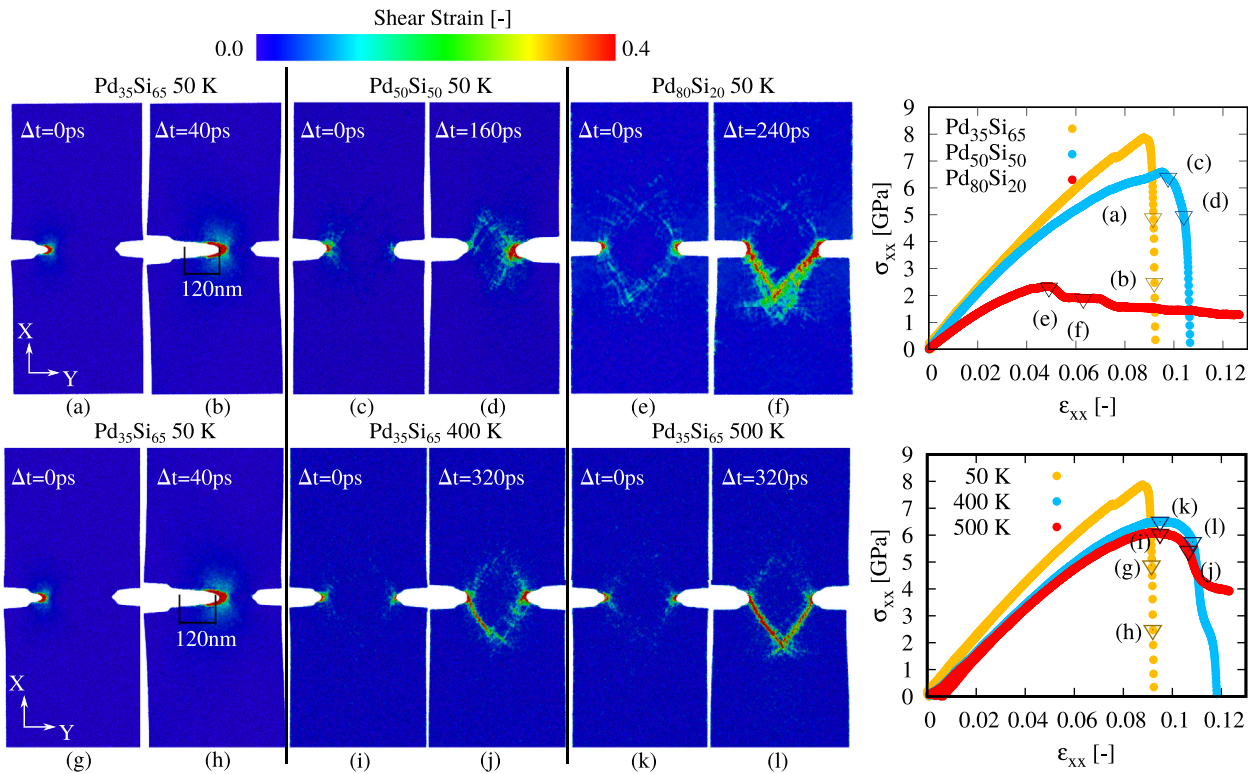


Fig. 3. Shear strain and σ - ϵ curves of notched PdSi samples deformed along the X-direction. (a-b) and (g-h): Pd₃₅Si₆₅ at 50 K shows cracking along the Y-direction and brittle failure. (c-d) and (i-j): Pd₅₀Si₅₀ at 50 K and Pd₃₅Si₆₅ at 400 K show a mixed deformation mode with cracking and emerging localized shearing. (e-f) and (k-l): Pd₈₀Si₂₀ at 50 K and Pd₃₅Si₆₅ at 500 K show shear bands starting from both notches and a serrated stress strain curve in the region of plastic flow.

for extending the EAM potential that only consists of two-body terms with a three-body term for Si-Si that leads to effective angular-dependency of the interactions. On the other side, many-body terms are neglected for the mostly metallic Pd-Pd and Pd-Si interactions.

3.2. Effect of temperature and composition on the tensile deformation

Three notched samples have been prepared to investigate the effect of composition on the deformation behavior of amorphous Pd₃₅Si₆₅, Pd₅₀Si₅₀ and Pd₈₀Si₂₀. A brittle-to-ductile transition from cracking perpendicular to the loading direction to localized shear banding upon tensile loading was observed with decreasing silicon content (see Fig. 3). The rapid stress drop to zero in the σ - ϵ -curves (see Fig. 3) of Pd₃₅Si₆₅ and Pd₅₀Si₅₀ indicates catastrophic failure. The brittleness of Pd₃₅Si₆₅ (Fig. 3(a–b)) is caused here by the formation of a sharp crack along the y-direction starting from the notch. The crack propagates at a speed of 3000 m/s, which is about the speed of sound in the material [36], and cleaves the sample. Some plastic strain is observed when the Si content decreases for Pd₅₀Si₅₀ (Fig. 3 (c–d)). The emerging plasticity in Pd₅₀Si₅₀ is revealed by the formation of shear bands at the notch tip and flattening in the stress-strain curve before reaching the ultimate tensile stress (UTS). Eventually, shear band propagation slows down and a fracture arises perpendicular to the loading direction, leading to the stress drop after the UTS. In contrast to the catastrophic failure observed in the two previous systems, Pd₈₀Si₂₀ shows a serrated plastic flow and localized shear banding (Fig. 3 (e–f)). The reason for this serrated flow is a repetitive stopping and starting of the shear banding process upon loading with constant strain rate [37]. Here, the shear bands start from both notches and propagate through the sample. The prevailing plastic deformation also significantly affects the strength of the MG. The UTS is also gradually decreasing from 8 GPa to 6 GPa and finally to 2 GPa by reducing the Si content from 65% to 50% and 20%, respectively. The UTS for

Pd₃₅Si₆₅ is resistance against interatomic rupture and, therefore, equivalent to the fracture strength. For Pd₅₀Si₅₀ and Pd₈₀Si₂₀, yielding set in before the fracture limit is reached. The elongation at fracture is about 10% for Pd₅₀Si₅₀ and Pd₃₅Si₆₅. In contrast, the yield point of Pd₈₀Si₂₀ lies at about 4%. Also in the fully-reversible elastic regime effects can be seen, where all samples relax back to their initial dimensions when removing the loading before reaching the UTS. A lower silicon content softens the MG and leads to a deviation of the σ - ϵ -curves from the linear elastic behavior. Nonlinear elastic effects originate from reversible atomic-level changes which are contributing to the elasticity stemming from changes in bond distance.

Interestingly, a similar transition to plasticity through shear banding can be induced in the brittle Pd₃₅Si₆₅ glass by gradually increasing the temperature from 50 K to 500 K. As mentioned above, cracking occurs at 50 K, while 400 K marks a transition point for the deformation behavior. A mixed deformation of shear banding and cracking occurs at 400 K (Fig. 3 (i–j)) that is similar to the deformation mechanism observed for Pd₅₀Si₅₀ at 50 K. Initially, a blunt crack starts to propagate from the notch. Then, at the left notch (Fig. 3 (i–j)) shear banding initiates, whereas on the right notch the crack still continues to grow. This will finally result in catastrophic failure. The specimen deforms only by the formation of localized narrow shear bands that nucleate at the notch when further increasing the temperature to 500 K. The propagation angle is around 45 degrees to the loading direction. The deformation behavior closely resembles the one observed for Pd₈₀Si₂₀ glass deformed at 50 K, except for the much higher UTS.

We also investigated the isothermal elastic properties for different compositions and temperatures, because of the well-known correlation between elastic and plastic properties of MGs. Areas of locally low shear modulus show early plastic deformation [38] or the Poisson's ratio criterion of toughness in MG [39], to name two striking examples. Indeed, a decrease in the silicon content and an increase in the temperature cause not only a decrease of the strength, but also elastic

Table 2

Elastic constants of Pd₈₀Si₂₀ and Pd₃₅Si₆₅. *G* and *B* obtained from sampling the stress change upon straining.

Metallic Glass	T [K]	B [GPa]	G [GPa]	ν [-]
Pd ₃₅ Si ₆₅	50	186.3	44.3	0.38
Pd ₃₅ Si ₆₅	500	168.0	34.4	0.41
Pd ₈₀ Si ₂₀	50	165.2	33.0	0.41

softening. However, the elastic properties are not changed uniformly (Table 2). The bulk modulus *B* and the shear modulus *G* are reduced by 10% and 20%, respectively, in Pd₈₀Si₂₀ at 50 K and Pd₃₅Si₆₅ at 500 K compared to Pd₃₅Si₆₅ at 50 K. This means that the Poisson's ratio ν will increase as well since the Poisson's ratio is connected to *B* and *G* by $\nu = \frac{3B-2G}{2(3K+G)}$. Thus, the obtained elastic properties are in agreement with the findings from experiments [40] and simulation [41], where the enhanced ductility was associated with an increase in Poisson's ratio.

3.3. Atomistic deformation mechanism of PdSi glass

Recently, Şopu et al. [42,43] proposed an atomic mechanism for shear band nucleation and propagation based on chained shear transformation zones (STZ) and vortices based on MD results. These two units can be identified by analyzing the rotational part of the deformation gradient tensor, which is obtained from a decomposition of the deformation gradient tensor into the rotation matrix and the right stretch tensor. STZs in the vicinity of the notch tip are activated by the displacement of the atoms in Pd₃₅Si₆₅ at 500 K (Fig. 4 (b)), as well as in Pd₈₀Si₂₀ at 50K (Fig. 4 (c)). The connected vortex activates the next STZ and the shear band starts to propagate through the sample. However, the atomic displacement at the notch tip does not lead to such STZ activation in Pd₃₅Si₆₅ at 50 K (Fig. 4 (a)). Instead, the high stress level at the notch tip triggers breaking of atomic bonds and a crack perpendicular to the loading direction propagates through the sample (Fig. 4 (c)).

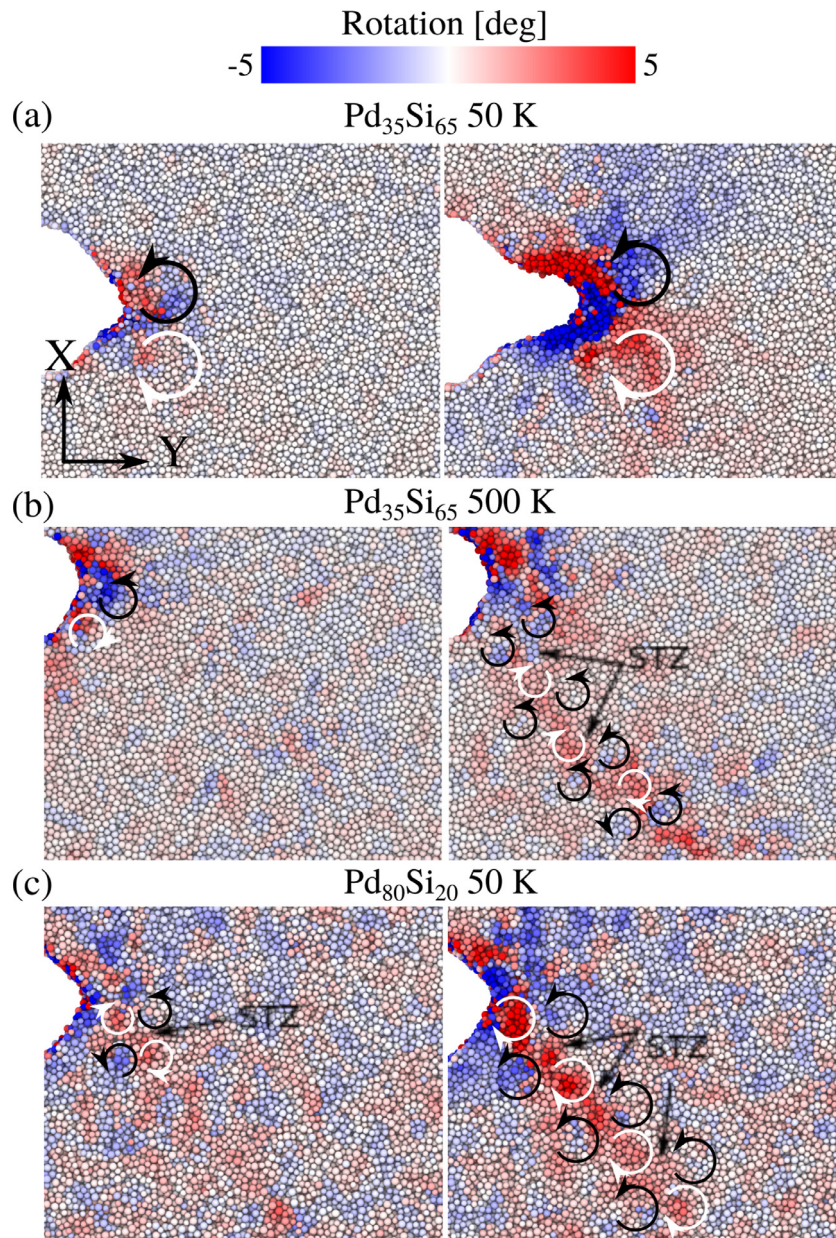


Fig. 4. Atomic scale mechanism of shear band nucleation and cracking resolved by the rotational part of the deformation gradient tensor. (a): Pd₃₅Si₆₅ at 50 K shows huge rotational displacement at the crack tip, but no STZ activation in the vicinity. (b) and (c): In Pd₃₅Si₆₅ at 500 K and Pd₈₀Si₂₀ at 50 K the rotational displacements of the atoms lead to STZ activation and localized plasticity.

Generally, the local barrier for STZ activation is influenced by the local order [8,44], bonding, local softening [45], free volume [46] and the relaxation state [47] of the metallic glass. Energetic barriers for STZ activation can be overcome by local stresses and thermal vibrations. The above-mentioned transition from cracking to shear banding can be explained by analyzing the spatial distribution of atomic level stresses across the sample and in particular at the notch tip. In general, the Tresca stress becomes more widely distributed when increasing the temperature or decreasing the silicon content (Fig. 5 (b.I–III)). The stress in Pd₃₅Si₆₅ at 50 K is accumulated around the notch tip and causes the rupture of bonds ahead of this tip. The rupturing of bonds further sharpens the notch and leads to an even more severe stress accumulation, which will eventually drive the crack further. In contrast, the stress shows a more broadened spatial distribution with fewer higher peaks for Pd₃₅Si₆₅ at 500 K and Pd₈₀Si₂₀ at 50 K. The overall Tresca stress at elevated temperature and increasing silicon is higher due to the virial contribution of kinetic energy to the stress and the higher amount of angular contributions of the interatomic interactions, respectively. Thermally-activated stress redistribution takes place during the loading and has to be, therefore, activated at picosecond timescale. The activation barrier for such

frequent events needs to be small. Estimation using a Boltzmann factor suggests energies around 0.1 eV. The only possible mechanisms with small enough energy barriers is stress redistribution by locally rearranging the atoms. On the other side, the activation energies of diffusion and STZ activation should be about 1–5 eV [48], and would therefore occur too rarely to effectively change the local stress state thermally in most parts of the sample during deformation.

The local rearrangements also affect the atomic volume, which is a measure for strain on the atomic scale. Thus, the local structure was analyzed in terms of a spatial average atomic volume obtained from the Voronoi tessellation in order to reinforce the rearrangement hypothesis. Because the Voronoi tessellation does not lead to meaningful results at the surface, these were not included in the analysis. Fig. 5 (a.I–III) shows the temperature and the composition effect on the spatial average of the atomic volume. Areas with high atomic volume are primarily located closely around the notch tip in Pd₃₅Si₆₅ at 50 K (Fig. 5 (a.I)). On the other hand Pd₃₅Si₆₅ at 500 K and Pd₈₀Si₂₀ deformed at 50 K (Fig. 5 (a.II–III)) display a broad spatial distribution of the atomic volume. The distribution and localization of the atomic volume correlate with the atomic level stress. Consequently, atomic rearrangement reduces the magnitude of atomic level stress and strain, respectively.

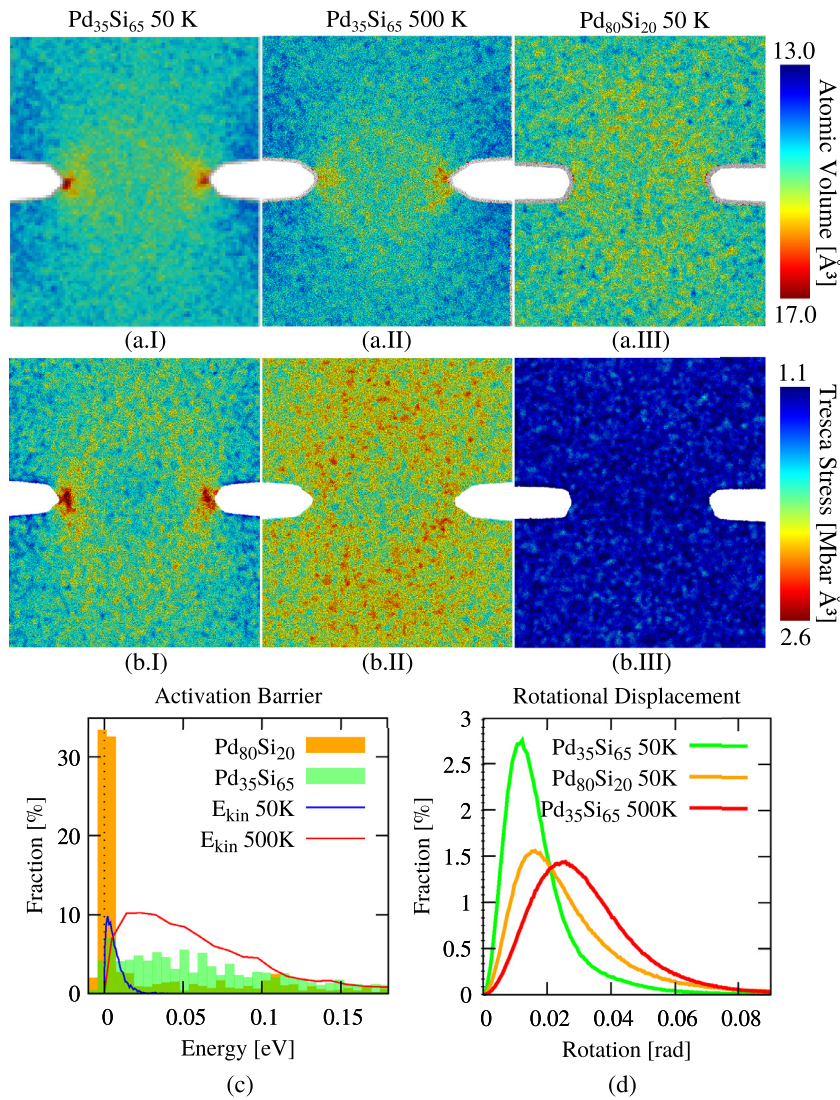


Fig. 5. Atomic volume and Tresca stress before the yield point. (a.I) and (b.I): Pd₃₅Si₆₅ at 50 K shows stress accumulation at the notch tip and a high local atomic volume. (a.II–III) and (b.II–III): Pd₃₅Si₆₅ at 500 K and Pd₈₀Si₂₀ at 50 K show evenly distributed atomic volume and Tresca stress. The overall Tresca stress at 500 K is higher due to the virial contribution of kinetic energy to the stress. Moreover, the overall Tresca stress in Pd₃₅Si₆₅ is higher than in Pd₈₀Si₂₀ due to the higher amount of angular contributions of the interatomic interactions. (c): Histogram of activation energies and average kinetic energy per atom obtained from a saddle point search of the potential energy landscape. Activation energies connected to events with displacements larger than 0.1 Å were considered. (d): Histogram of rotational displacement of groups of atoms during deformation.

The accommodation of macroscopic strain is not only due to the change of the bonding distances but also to structural reorientations. Moreover, a correlation between the microscopic stress redistribution and the macroscopic shear modulus is observed as well. The reduced shear modulus at higher temperatures and lower silicon contents enable easier accommodation of the deformation due to local shearing. These macroscopic shearing events result in a local rotational displacement of groups of atoms. The effect of thermal activation and composition on this reorientation can be seen by comparing the rotational displacements of groups of atoms (Fig. 5 (d)). At higher temperatures (Fig. 4 (b)) and low Si (Fig. 4 (c)) contents, small spatial regions of rotations can be seen across the sample, while at low temperature the rotations in the regions away from the notch are almost zero (Fig. 4 (a)). However, rotational rearrangements involving up to 50 atoms leave the atomic bond angle distribution almost unchanged (see Fig. A2); only the Si-Si bond angles show some broadening. A lack of local atomic rearrangements will cause stress accumulation at the notch and eventually fracture by bond breaking. On the other hand, these local rotations are, therefore, the prerequisite for STZs and, ultimately, also for plasticity through shear banding.

In our case, 400 K for Pd₃₅Si₆₅ or a Si content of 50% at 50 K marks a transition point from predominately brittle cracking to plasticity through shear banding. At the early stage of deformation, the redistribution of the stress is not strong enough and a crack is initiated. At an elevated temperature or a low silicon content STZs can be still activated, which, in turn, leads to a complex deformation process consisting of shear banding and cracking.

A quantitative assessment of the local relaxations can be performed by sampling the energy barrier distribution as a function of the composition. The activation barrier energy is the difference between the energy of the initial minimum and the saddle point position. It is the energy barrier that needs to be overcome to move the system into an adjacent energy minimum position. In the case of a dense system, these moves are typically local with one or a few atoms moving over distances to a maximum of a near-neighbor distance. Displacements of atoms at around 0.1 to 0.5 Å and energies of 0.1 eV correspond to local structural rearrangements, whereas events with bigger displacements and energies around 1 to 5 eV can be identified as diffusional jumps. The ART simulations also converge towards a few barriers with energies slightly lower than the initial state by -0.001 eV to 0.0 eV. These are positioned as a small distance from the initial state, around 0.1 Å. These small displacements suggest very limited atomic movement and a small state change. The presence of pseudo-events indicate either a relatively energetically flat region around the minimum or a relatively rough landscape. In the first case, no barrier exists between the two points and this suggests that

the convergence criteria for minimizing the energy were not strict enough to bring the system to the exact local minimum. In the second case, the roughness is generally linked to configurations that are still very energetic, with considerable strain still present; because minima are very close to each other (less than 0.1 Å), they can be missed by the algorithm. Since these features are washed out kinetically, even at very low temperature, their presence in this simulation does not affect the overall results presented here. We note, in particular, that this observation depends on the system studied, the specific implementation of the method and the selection of parameters, which explains why these have not been reported in other studies with EAM [10,49] or Lennard-Jones potentials [50,51].

These histograms of activation barriers are known to be correlated to the local order and structure in MGs [10]. For Pd₈₀Si₂₀, the activation energies are narrowly distributed around 0 eV, while Pd₃₅Si₆₅ shows a much wider distribution (see Fig. 5 (c)). The probability of thermal activation can be estimated by comparing to the distribution of the kinetic energies per atom at 50 K and 500 K in the samples. One can see that 33% of the activation barriers are higher than 0.01 eV in Pd₈₀Si₂₀, whereas in Pd₃₅Si₆₅ the percentage is above 89%. At 50 K, less than 10% of the atoms have more than 0.01 eV kinetic energy per atom, while at 500 K 81% of the atoms have more than 0.01 eV. Thermal activation of local relaxation events will, therefore, be more likely in Pd₈₀Si₂₀ than in Pd₃₅Si₆₅. This provides a quantitative assessment of the observed differences in the distribution of rotations, stress and atomic strain. At low activation barriers the atoms can easily rearrange, while the bond angles are preserved during these relaxations. The atoms will show collective rotative motion and accommodate the externally applied strain. The stress level will not reach the fracture strength at which bonds are rupturing, when thermally-activated relaxation is possible.

3.4. Crack propagation

Generally, brittle fracture involves the break of interatomic bonds ahead of the crack tip at the atomic level. The crack path is strongly influenced by the local structural properties, local stress state and by elastic inhomogeneities of the material. In covalently-bonded nonmetallic glasses the rigidity of the bonding leads to a perfectly sharp crack [52], similar to the one observed here for Pd₃₅Si₆₅ deformed at 50 K. Experimentally, the fracture surface of MGs shows periodic corrugation that suggests crack propagation through nanoscale void formation. This corrugated fracture patterns coarsen in more ductile MG [53]. Void formation and fracture are suspected to be closely related to structural fluctuations and the configuration of brittle heterogeneities [54]. In our case, crack deflection and formation of voids is evoked by using a more inhomogeneous sample material in the simulation (see Fig. 6).

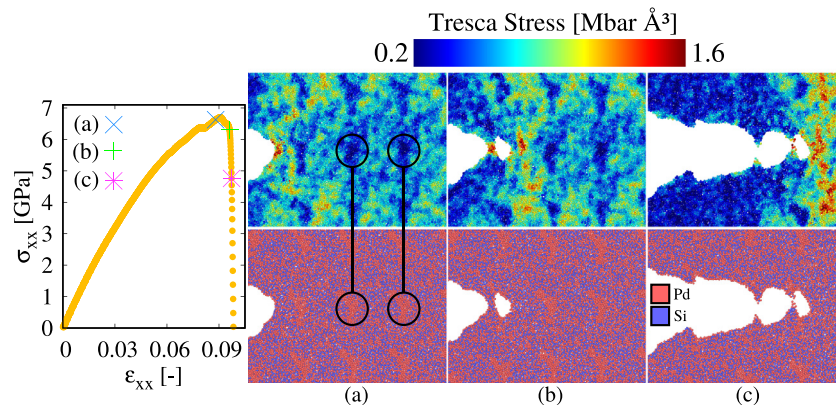


Fig. 6. Crack propagation through void nucleation ahead of the crack tip in an inhomogeneous amorphous Pd₅₀Si₅₀ alloy at 50K and the corresponding stress-strain curve. Pd precipitations (black circle) show low Tresca stresses due to easy local relaxation. (a) blunting of notch tip. (b) Void nucleation ahead of the crack tip. (c) Fracture surface with ruptured bridges.

Specifically, a Pd₅₀Si₅₀ alloy with an inhomogeneous glassy structure that formed small Pd and Si precipitates during quenching was used. Upon loading, the crack initiates at the notch and starts to propagate by void formation ahead of the crack tip following areas of Pd precipitations. These Pd precipitations create a weak path, where bond rupture can easily occur. The Tresca stress in these Pd accumulation is significantly lower than in the bulk (see Fig. 6 (black circle)). In these areas local relaxations is easily possible due to the absence of rigid covalently-bonded network of Si-Si atoms, which in turn also lead to stress relaxation. In contrast, the stress accumulates in more homogeneous bulk areas with an interconnected covalent Si-Si bond network. When the stress field ahead of the crack tip reaches the weaker Pd accumulations, atoms will shear severely and interatomic bonds will rupture. The relatively soft and weak Pd accumulations cannot withstand this local loading. Eventually, there will be decohesion of the material and a void will form. The small material bridge between the initial crack tip and the growing void will rupture too. The resulting fracture surface shows then the experimentally found corrugations [55].

4. Summary and conclusions

In summary, a brittle-to-ductile transition in the tensile deformation behavior of metal-metalloid PdSi glasses can arise through the increase of the temperature or the decrease in the silicon content. A decrease in silicon content leads to fewer covalent bonds and, therefore, lower activation barriers that facilitates local relaxation through atomic rearrangements. These local relaxations lead to stress redistribution still in the elastic loading regime and are the precursor of the STZs activation. The STZ will lead ultimately to plasticity in the form of shear bands. On the other side, at too low temperature these barrier cannot be overcome and cracking will dominate over shear banding. In this case, high activation barriers for local relaxation impedes stress redistribution at the notch tip and there will be decohesion of the material. Additionally, the cracking path also depends on the degree of homogeneity. In particular, a corrugated fracture surface similar to experiment can be formed due to crack deflection and cavitation ahead of the notch tip in chemically inhomogeneous samples. In contrast, a sharp cleavage-like fracture occurs for more homogeneous samples.

Data availability

The data that support the findings of this study are available from the corresponding author upon reasonable request.

Declaration of Competing Interest

The authors declare that they have no known competing financial interests or personal relationships that could have appeared to influence the work reported in this paper.

CRediT authorship contribution statement

F. Moitzi: Conceptualization, Formal analysis, Writing - original draft, Writing - review & editing. **D. Šopu:** Conceptualization, Supervision, Writing - original draft, Writing - review & editing. **D. Holec:** Data curation, Writing - review & editing. **D. Perera:** Data curation, Writing - review & editing. **N. Mousseau:** Data curation, Writing - review & editing. **J. Eckert:** Conceptualization, Supervision, Writing - review & editing.

Acknowledgment

Financial support through the European Research Council under the Advanced Grant INTELHYB (grant ERC-2013-ADG-340025) and Deutsche Forschungsgemeinschaft (DFG) (Grant no. SO 1518/1-1) is gratefully acknowledged. Calculations for this research were conducted on the

Lichtenberg high performance computer of the Technische Universität Darmstadt and the high performance cluster in Leoben. The authors are grateful for the discussions with Prof. Joachim Wittmer, ICS Strassbourg about the evaluation of isothermal elastic constants in amorphous systems and thank Ulrike Nitzsche for technical assistance concerning the computer simulations.

Supplementary material

Supplementary material associated with this article can be found in the online version at doi:10.1016/j.actamat.2020.02.002.

References

- [1] M. Jafary-Zadeh, G. Praveen Kumar, P.S. Branicio, M. Seifi, J.J. Lewandowski, F. Cui, A critical review on metallic glasses as structural materials for cardiovascular stent applications, *J. Funct. Biomater.* 9 (1) (2018), doi: 10.3390/jfb9010019.
- [2] Z.F. Zhang, J. Eckert, L. Schultz, Difference in compressive and tensile fracture mechanisms of Zr₅₉Cu₂₀Al₁₀Ni₈Ti₃ bulk metallic glass, *Acta Mater.* 51 (4) (2003) 1167–1179, doi: 10.1016/s1359-6454(02)00521-9.
- [3] X.D. Wang, J. Bednarcik, K. Saks, H. Franz, Q.P. Cao, J.Z. Jiang, Tensile behavior of bulk metallic glasses by in situ x-ray diffraction, *Appl. Phys. Lett.* 91 (8) (2007) 81913, doi: 10.1063/1.2773945.
- [4] C. Schuh, T. Hufnagel, U. Ramamurty, Mechanical behavior of amorphous alloys, *Acta Mater.* 55 (12) (2007) 4067–4109, doi: 10.1016/j.actamat.2007.01.052.
- [5] D. Wei, J. Yang, M.-Q. Jiang, B.-C. Wei, Y.-J. Wang, L.-H. Dai, Revisiting the structure–property relationship of metallic glasses: common spatial correlation revealed as a hidden rule, *Phys. Rev. B* 99 (2019) 014115–014128, doi: 10.1103/PhysRevB.99.014115.
- [6] A. Hirata, P. Guan, T. Fujita, Y. Hirotsu, A. Inoue, A.R. Yavari, T. Sakurai, M. Chen, Direct observation of local atomic order in a metallic glass, *Nat. Mater.* 10 (1) (2010) 28–33, doi: 10.1038/nmat2897.
- [7] H.Y. Xu, M.Z. Li, Activation-relaxation technique study on beta-relaxation in La₅₅Ni₂₀Al₂₅ and Cu₄₆Zr₄₆Al₈ metallic glasses, *Intermetallics* 94 (2018) 10–16, doi: 10.1016/j.intermet.2017.12.017.
- [8] Y. Ritter, K. Albe, Chemical and topological order in shear bands of Cu₆₄Zr₃₆ and Cu₃₆Zr₆₄ glasses, *J. Appl. Phys.* 111 (10) (2012) 103527, doi: 10.1063/1.4717748.
- [9] C.-X. Peng, D. Šopu, K.-K. Song, Z.-T. Zhang, L. Wang, J. Eckert, Bond length deviation in CuZr metallic glasses, *Phys. Rev. B* 96 (17) (2017) 174112.
- [10] J. Ding, Y.-Q. Cheng, H. Sheng, M. Asta, R.O. Ritchie, E. Ma, Universal structural parameter to quantitatively predict metallic glass properties, *Nat. Commun.* 7 (1) (2016) 13733, doi: 10.1038/ncomms13733.
- [11] X.K. Xi, D.Q. Zhao, M.X. Pan, W.H. Wang, Y. Wu, J.J. Lewandowski, Fracture of brittle metallic glasses: brittleness or plasticity, *Phys. Rev. Lett.* 94 (12) (2005) 125510–125513, doi: 10.1103/physrevlett.94.125510.
- [12] P. Murali, T.F. Guo, Y.W. Zhang, R. Narasimhan, Y. Li, H.J. Gao, Atomic scale fluctuations govern brittle fracture and cavitation behavior in metallic glasses, *Phys. Rev. Lett.* 107 (2011) 215501–215506, doi: 10.1103/PhysRevLett.107.215501.
- [13] Y. He, P. Yi, M.L. Falk, Critical analysis of an FeP empirical potential employed to study the fracture of metallic glasses, *Phys. Rev. Lett.* 122 (2019) 35501–35506, doi: 10.1103/PhysRevLett.122.035501.
- [14] E. Park, D. Kim, Phase separation and enhancement of plasticity in Cu–Zr–Al–Y bulk metallic glasses, *Acta Mater.* 54 (10) (2006) 2597–2604, doi: 10.1016/j.actamat.2005.12.020.
- [15] H.W. Sheng, M.J. Kramer, A. Cadieu, T. Fujita, M.W. Chen, Highly optimized embedded-atom-method potentials for fourteen fcc metals, *Phys. Rev. B* 83 (13) (2011), doi: 10.1103/physrevb.83.134118.
- [16] J. Tersoff, Empirical interatomic potential for silicon with improved elastic properties, *Phys. Rev. B* 38 (14) (1988) 9902–9905, doi: 10.1103/physrevb.38.9902.
- [17] N. Mousseau, L.K. Béland, P. Brommer, J.-F. Joly, F. El-Mellouhi, E. Machado-Charry, M. Marinica, P. Pochet, The activation-relaxation technique: art nouveau and kinetic art, *J. Atomic Mol. Opt. Phys.* 2012 (2012) 1–14, doi: 10.1155/2012/925278.
- [18] G.T. Barkema, N. Mousseau, Event-based relaxation of continuous disordered systems, *Phys. Rev. Lett.* 77 (21) (1996) 4358–4361, doi: 10.1103/physrevlett.77.4358.
- [19] R. Malek, N. Mousseau, Dynamics of Lennard-Jones clusters: a characterization of the activation-relaxation technique, *Phys. Rev. E* 62 (6) (2000) 7723–7728, doi: 10.1103/physreve.62.7723.
- [20] V. Schnabel, B.N. Jaya, M. Koehler, D. Music, C. Kirchlechner, G. Dehm, D. Raabe, J.M. Schneider, Electronic hybridisation implications for the damage-tolerance of thin film metallic glasses, *Sci. Rep.* 6 (1) (2016), doi: 10.1038/srep36556.
- [21] S. Plimpton, Fast parallel algorithms for short-range molecular dynamics, *J. Comput. Phys.* 117 (1) (1995) 1–19, doi: 10.1006/jcph.1995.1039.
- [22] D. Šopu, Y. Ritter, H. Gleiter, K. Albe, Deformation behavior of bulk and nanostructured metallic glasses studied via molecular dynamics simulations, *Phys. Rev. B* 83 (10) (2011) 100202, doi: 10.1103/PhysRevB.83.100202.
- [23] M.J. Mees, G. Pourtois, E.C. Neyts, B.J. Thijsse, A. Stesmans, Uniform-acceptance force-bias monte carlo method with time scale to study solid-state diffusion, *Phys. Rev. B* 85 (2012) 134301–134309, doi: 10.1103/PhysRevB.85.134301.
- [24] A. Foroughi, H. Ashuri, R. Tavakoli, M. Stoica, D. Šopu, J. Eckert, Structural modification through pressurized sub-T_g annealing of metallic glasses, *J. Appl. Phys.* 122 (21) (2017) 215106, doi: 10.1063/1.5004058.

- [25] Z. Sha, Y. Teng, L.H. Poh, Q. Pei, G. Xing, H. Gao, Notch strengthening in nanoscale metallic glasses, *Acta Mater.* 169 (2019) 147–154. <http://www.sciencedirect.com/science/article/pii/S1359645419301302>
- [26] D. Raut, R.L. Narayan, Y. Yokoyama, P. Tandaiya, U. Ramamurty, Fracture of notched ductile bulk metallic glass bars subjected to tension-torsion: experiments and simulations, *Acta Mater.* 168 (2019) 309–320. <http://www.sciencedirect.com/science/article/pii/S1359645419301119>
- [27] G. Gao, K. Van Workum, D. Schall, J. Harrison, Elastic constants of diamond from molecular dynamics simulations, *J. Phys. Condens. Matter.* 18 (32) (2006) 1737–1750, doi: [10.1088/0953-8984/18/32/s05](https://doi.org/10.1088/0953-8984/18/32/s05).
- [28] A. Stukowski, Visualization and analysis of atomistic simulation data with Ovito—the open visualization tool, *Model. Simul. Mater. Sci. Eng.* 18 (1) (2010) 15012, doi: [10.1088/0965-0393/18/1/015012](https://doi.org/10.1088/0965-0393/18/1/015012).
- [29] M.J. Soler, E. Artacho, J.G. Gale, A. García, J. Junquera, P. Ordejón, S. Sánchez-Portal, The SIESTA method for ab initio order-N materials simulation, *J. Phys. Condens. Matter* 14 (11) (2002) 2745–2779, doi: [10.1088/0953-8984/14/11/302](https://doi.org/10.1088/0953-8984/14/11/302).
- [30] J.P. Perdew, K. Burke, M. Ernzerhof, Generalized gradient approximation made simple, *Phys. Rev. Lett.* 77 (1996) 3865–3868, doi: [10.1103/PhysRevLett.77.3865](https://doi.org/10.1103/PhysRevLett.77.3865).
- [31] M. Krack, Pseudopotentials for h to Kr optimized for gradient-corrected exchange-correlation functionals, *Theor. Chem. Acc.* 114 (1–3) (2005) 145–152, doi: [10.1007/s00214-005-0655-y](https://doi.org/10.1007/s00214-005-0655-y).
- [32] R. Dronskowski, P.E. Blochl, Crystal orbital hamilton populations (COHP): energy-resolved visualization of chemical bonding in solids based on density-functional calculations, *J. Phys. Chem.* 97 (33) (1993) 8617–8624, doi: [10.1021/j100135a014](https://doi.org/10.1021/j100135a014).
- [33] A.H. Larsen, J. Mortensen, J. Blomqvist, The atomic simulation environment—a python library for working with atoms, *J. Phys. Condens. Matter* 29 (27) (2017) 273002.
- [34] A. Kokalj, XCrySDen—a new program for displaying crystalline structures and electron densities, *J. Mol. Gr. Model.* 17 (3–4) (1999) 176–179, doi: [10.1016/s1093-3263\(99\)00028-5](https://doi.org/10.1016/s1093-3263(99)00028-5).
- [35] V. Schnabel, M. Köhler, D. Music, J. Bednarcik, W.J. Clegg, D. Raabe, J.M. Schneider, Ultra-stiff metallic glasses through bond energy density design, *J. Phys. Condens. Matter* 29 (26) (2017) 265502, doi: [10.1088/1361-648x/aa72cb](https://doi.org/10.1088/1361-648x/aa72cb).
- [36] D. Crespo, P. Bruna, A. Valles, E. Pineda, Phonon dispersion relation of metallic glasses, *Phys. Rev. B* 94 (2016) 144205, doi: [10.1103/PhysRevB.94.144205](https://doi.org/10.1103/PhysRevB.94.144205).
- [37] D. Şöpu, A. Foroughi, M. Stoica, J. Eckert, Brittle-to-ductile transition in metallic glass nanowires, *Nano Lett.* 16 (2016) 4467–4471.
- [38] N. Wang, J. Ding, F. Yan, M. Asta, R.O. Ritchie, L. Li, Spatial correlation of elastic heterogeneity tunes the deformation behavior of metallic glasses, *NPJ Comput. Mater.* 4 (1) (2018) 19, doi: [10.1038/s41524-018-0077-8](https://doi.org/10.1038/s41524-018-0077-8).
- [39] J.J. Lewandowski, A.L. Greer, Temperature rise at shear bands in metallic glasses, *Nat. Mater.* 5 (1) (2005) 15–18, doi: [10.1038/nmat1536](https://doi.org/10.1038/nmat1536).
- [40] T.-W. Wu, F. Spaepen, The relation between embrittlement and structural relaxation of an amorphous metal, *Philos. Mag. B* 61 (4) (1990) 739–750, doi: [10.1080/13642819008219307](https://doi.org/10.1080/13642819008219307).
- [41] C.-Y. Wu, Y.-C. Wang, Indentation behavior of metallic glass via molecular dynamics simulation, *Handbook of Mechanics of Materials*, 2018, pp. 1–14, doi: [10.1007/978-981-10-6855-3_2-1](https://doi.org/10.1007/978-981-10-6855-3_2-1).
- [42] D. Şöpu, A. Stukowski, M. Stoica, S. Scudino, Atomic-level processes of shear band nucleation in metallic glasses, *Phys. Rev. Lett.* 119 (2017) 195503–195507, doi: [10.1103/PhysRevLett.119.195503](https://doi.org/10.1103/PhysRevLett.119.195503).
- [43] D. Şöpu, S. Scudino, X.L. Bian, C. Gammer, J. Eckert, Atomic-scale origin of shear band multiplication in heterogeneous metallic glasses, *Scr. Mater.* 178 (2020) 57–61.
- [44] T. Brink, K. Albe, From metallic glasses to nanocrystals: molecular dynamics simulations on the crossover from glass-like to grain-boundary-mediated deformation behaviour, *Acta Mater.* 156 (2018) 205–214, doi: [10.1016/j.actamat.2018.06.036](https://doi.org/10.1016/j.actamat.2018.06.036).
- [45] Y.Q. Cheng, A.J. Cao, H. Sheng, E. Ma, Local order influences initiation of plastic flow in metallic glass: effects of alloy composition and sample cooling history, *Acta Mater.* 56 (18) (2008) 5263–5275, doi: [10.1016/j.actamat.2008.07.011](https://doi.org/10.1016/j.actamat.2008.07.011).
- [46] L. Li, E. Homer, C. Schuh, Shear transformation zone dynamics model for metallic glasses incorporating free volume as a state variable, *Acta Mater.* 61 (9) (2013) 3347–3359, doi: [10.1016/j.actamat.2013.02.024](https://doi.org/10.1016/j.actamat.2013.02.024).
- [47] A. Barbot, M. Lerbinger, A. Hernandez-García, R. García-García, M.L. Falk, D. Vandembroucq, S. Patinet, Local yield stress statistics in model amorphous solids, *Phys. Rev. E* 97 (2018) 33001–33013, doi: [10.1103/PhysRevE.97.033001](https://doi.org/10.1103/PhysRevE.97.033001).
- [48] F. Faupel, W. Frank, M. Macht, H. Mehrer, V. Naundorf, K. Raetzke, H. Schober, S. Sharma, H. Teichler, Diffusion in metallic glasses and supercooled melts, *Rev. Mod. Phys.* 75 (2003) 237–280, doi: [10.1103/RevModPhys.75.237](https://doi.org/10.1103/RevModPhys.75.237).
- [49] Y. Fan, T. Iwashita, T. Egami, Energy landscape-driven non-equilibrium evolution of inherent structure in disordered material, *Nat. Commun.* 8 (1) (2017) 15417, doi: [10.1038/ncomms15417](https://doi.org/10.1038/ncomms15417).
- [50] D. Rodney, C. Schuh, Distribution of thermally activated plastic events in a flowing glass, *Phys. Rev. Lett.* 102 (23) (2009) 235503.
- [51] D. Rodney, C.A. Schuh, Yield stress in metallic glasses: the Jamming-Unjamming transition studied through monte carlo simulations based on the activation-relaxation technique, *Phys. Rev. B* 80 (18) (2009) 184203, doi: [10.1103/PhysRevB.80.184203](https://doi.org/10.1103/PhysRevB.80.184203).
- [52] J.M. Rimsza, R.E. Jones, L.J. Criscenti, Crack propagation in silica from reactive classical molecular dynamics simulations, *J. Am. Ceram. Soc.* 101 (4) (2017) 1488–1499, doi: [10.1111/jace.15292](https://doi.org/10.1111/jace.15292).
- [53] R. Raghavan, P. Murali, U. Ramamurty, On factors influencing the ductile-to-brittle transition in a bulk metallic glass, *Acta Mater.* 57 (11) (2009) 3332–3340, doi: [10.1016/j.actamat.2009.03.047](https://doi.org/10.1016/j.actamat.2009.03.047).
- [54] P. Murali, U. Ramamurty, V.B. Shenoy, Factors influencing deformation stability of binary glasses, *J. Chem. Phys.* 128 (10) (2008) 104508, doi: [10.1063/1.2839300](https://doi.org/10.1063/1.2839300).
- [55] M.Q. Jiang, Z. Ling, J.X. Meng, L.H. Dai, Energy dissipation in fracture of bulk metallic glasses via inherent competition between local softening and quasi-cleavage, *Philos. Mag.* 88 (3) (2008) 407–426, doi: [10.1080/14786430701864753](https://doi.org/10.1080/14786430701864753).